Phase Behavior and Rheological Analysis of Reverse Liquid Crystals and W/I-2 and W/H-2 Gel Emulsions Using an Amphiphilic Block Copolymer

ARTICLE *in* LANGMUIR · FEBRUARY 2011

Impact Factor: 4.46 · DOI: 10.1021/la104539q · Source: PubMed

3 AUTHORS, INCLUDING:

Anna May-Masnou
Materials Science Institute of Barcelona
10 PUBLICATIONS **81** CITATIONS
SEE PROFILE

José María Gutiérrez
University of Barcelona
47 PUBLICATIONS **1,177** CITATIONS
SEE PROFILE

Langmuir

ARTICLE

pubs.acs.org/Langmuir

Phase Behavior and Rheological Analysis of Reverse Liquid Crystals and W/I_2 and W/H_2 Gel Emulsions Using an Amphiphilic Block Copolymer

Anna May,*[,†] Kenji Aramaki,[‡] and José María Gutiérrez[†]

[†]Chemical Engineering Department, Chemistry Faculty, Barcelona University, Marti i Franquès 1-11, 08028, Barcelona, Catalonia, Spain

[‡]Graduate School of Environment and Information Sciences, Yokohama National University, Tokiwadai 79-7, Hodogaya-ku, Yokohama 240-8501, Japan

Supporting Information

ABSTRACT: This article reports the phase behavior determination of a system forming reverse liquid crystals and the formation of novel disperse systems in the two-phase region. The studied system is formed by water, cyclohexane, and Pluronic L-121, an amphiphilic block copolymer considered of special interest due to its aggregation and structural properties. This system forms reverse cubic (I_2) and reverse hexagonal (H_2) phases at high polymer concentrations. These reverse phases are of particular interest since in the two-phase region, stable high internal phase reverse emulsions can be formed. The characterization of the I_2 and H_2 phases and of the derived gel emulsions was performed with small-angle X-ray scattering (SAXS) and rheometry, and the influence of temperature and water content was studied. The H_2 phase experimented a thermal transition to an I_2 phase when temperature was increased, which presented an *Fd*3*m* structure. All samples showed a strong shear thinning behavior from low shear rates. The elastic modulus (G') in the I_2 phase was around 1 order of magnitude higher than in the H_2 phase. G' was predominantly higher than the viscous modulus (G''). In the gel emulsions, G' was nearly frequency-independent, indicating their gel type nature. Contrarily to water-in-oil (W/O) normal emulsions, in W/I_2 and W/H_2 gel emulsions, G', the complex viscosity ($|\eta^*|$), and the yield stress (τ_0) decreased with increasing water content, since the highly viscous microstructure of the continuous phase was responsible for the high viscosity and elastic behavior of the emulsions, instead of the volume fraction of dispersed phase and droplet size. A rheological analysis, in which the cooperative flow theory, the soft glass rheology model, and the slip plane model were analyzed and compared, was performed to obtain one single model that could describe the non-Maxwellian behavior of both reverse phases and highly concentrated emulsions and to characterize their microstructure with the rheological properties.

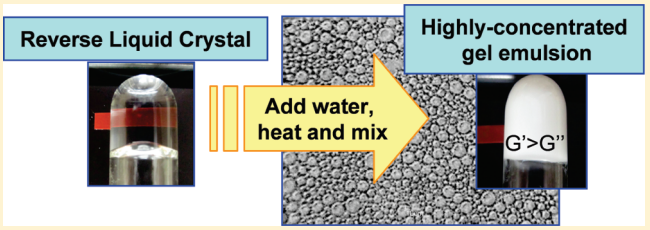

1. INTRODUCTION

Both highly concentrated emulsions,[1] also referred as high-internal-phase ratio emulsions (HIPRE), and emulsions with a structured mesophase (liquid crystal) in the continuous phase[2] are described by the term "gel emulsions", since they are both highly viscous emulsions. In this study, the term will be used mainly for the latter definition. These emulsions possess a finite yield stress, so they do not flow under their own weight[3] and they exhibit a non-Newtonian shear-thinning behavior.[4] They have been of great interest recently due to their intrinsic enhanced long-term stability, mainly due to the presence of the microstructured continuous phase, which prevents droplet coalescence as a result of its high viscosity.[5,6] A good review of this topic was performed by Rodríguez-Abreu and Lazzari.[7] This external microstructure has been reported to serve as an emulsion template for the preparation of meso/macroporous materials[8−11] as well as nanoparticles,[12] topics that are being widely researched since the first discovery in the early 1990s.[13]

Most studies regarding gel emulsions with a structured mesophase have been performed with systems that present a cubic liquid crystal in the continuous phase, direct (I_1)[2,14,15] or reverse (I_2).[6,16−18] Cubic phases are highly appreciated for being the most viscous and, therefore, good emulsion stabilizers. Among them, normal cubic-based emulsions (O/I_1), with oil as the dispersed phase, are more common, using nonionic surfactants based on poly(ethylene oxide) chains or ionic surfactants. The formation of I_1 phase is usually enhanced with the addition of oil. Reverse cubic-phase-based emulsions (W/I_2) are less studied due to the difficulty of finding surfactants to form a reverse structure. It could seem that the surfactants having a short chain length could form I_2 structures in a nonpolar phase, but their segregation tendency is not strong enough for aggregation in nonpolar medium.[16] Even if there are poly(oxyethylene) surfactants with a low hydrophilic−lipophlic balance (HLB) number, they would not be able to form these structures.[19] For that reason, a long-lipophilic chain surfactant should be used to form I_2.

Received: November 15, 2010
Revised: January 10, 2011
Published: February 02, 2011

Some of the amphiphilic substances that are used include copolymers like poly(oxyethylene)−poly(dimethylsiloxane) (HLB ∼ 5) or the several poly(oxyethylene)−poly(oxypropylene) type, which are known to form I_2 phase in the presence of water−oil mixtures.[17,20,21] Lecithin has also been reported to form an I_2 phase,[22] although due to its impurities, the phase diagram could vary from one system to another.

Gel emulsions with a direct hexagonal phase on the continuous phase, O/H_1, have been studied with a nonionic surfactant and several solvents;[15] also, emulsions with a lamellar phase in the continuous phase[23] and emulsions with a two-phase continuous phase consisting of a reverse hexagonal and lamellar phases ($H_2 + L_\alpha$) were formed in monoolein-based systems[5] up to 80 wt % of water. However, to our knowledge, there is no such study of gel emulsions with only the reverse hexagonal phase in the continuous phase (W/H_2), which would be placed between the ones with lamellar phase and cubic phase regarding stiffness and stability, and with an interesting microstructure to use as template for the formation of meso/macroporous materials. This research fills this existent gap of knowledge, apart from providing additional data regarding stability, rheology, and microstructure of the reverse liquid crystals and gel emulsions formed.

In this study, we have undertaken an analysis of the phase behavior of a new system, the water/Pluronic L 121/cyclohexane system, paying particular attention to the formation of reverse liquid crystals. We have investigated the ability of the system to form water-in-oil emulsions with a structured continuous phase (W/I_2 and W/H_2), and we have performed a thermal, rheological, and SAXS characterization of the one-phase regions and gel emulsions formed, studying the effect of water concentration and temperature. Precisely, we are interested in using this system to form highly concentrated reverse emulsions in order to produce, in a further study, meso/macroporous materials with high surface area and porosity, which will be able to increase diffusion and mass transfer in their potential applications.[10] This study is part of an ongoing far more complex study that will reach its culmination when all the process, from emulsion formation, rheological characterization, evolution during templating, and properties of the meso/macroporous materials will be fully described and characterized.

2. EXPERIMENTAL SECTION

2.1. Materials. The amphiphilic poly(ethylene glycol)-*block*-poly(propylene glycol)-*block*-poly(ethylene glycol), $(EO)_5(PO)_{68}(EO)_5$, triblock copolymer (Pluronic L 121 [P-121 from now on]) (M_w 4400 g/mol) was purchased from Sigma-Aldrich. This copolymer is hydrophobic, as the weight fraction of the hydrophobic PO chains is far more significant than the hydrophilic EO chains. It was chosen in order to form reverse liquid crystals. SAXS patterns of the pure block copolymer show no correlation peaks at low q values, which is an indication that it does not form aggregates without the presence of water or oil; a broad peak appears around 14 nm^{-1}, indicating the disordered liquidlike behavior of the polymer. Cyclohexane was provided from Tokyo Chemical Industry. All chemicals were used without further purification. Milli-Q deionized water was used in all samples.

2.2. Methods. *2.2.1. Determination of the Phase Behavior.* In order to determine the different regions of the phase diagram, the required amounts of the components were weighed in clean and dry glass tubes (ϕ = 13 mm). A proper mixing and homogenization of the samples was achieved using a vortex stirrer, together with heating of the samples in a dry thermo-bath combined with centrifugation. Once homogenization was attained, samples were kept in a water bath at 25 °C for several weeks to ensure that equilibrium was achieved. Visual observation, together with cross-polarizers, was used to identify the phases formed according to their stiffness and birefringence. Moreover, SAXS analysis was performed to confirm the liquid crystal phases formed and determine the phase boundaries.

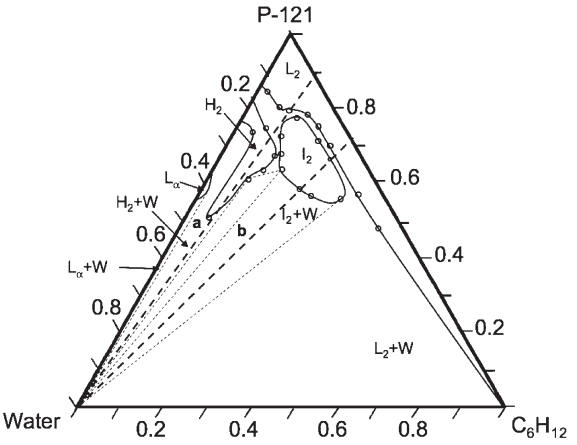

Figure 1. Phase diagram of the water/$(EO)_5(PO)_{68}(EO)_5$/C_6H_{12} system at 25 °C. Solid lines indicate the one-phase boundaries. Phases: L_α, lamellar; H_2, reverse hexagonal phase; I_2, reverse micellar cubic phase; L_2, reverse micellar solution. W indicates excess water. The two thick dashed lines, named **a** and **b**, are the water-addition paths followed in this study at a constant polymer/oil ratio: P/O = 90/10 in path **a** and P/O = 72.5/27.5 in **b**.

2.2.2. Preparation of Gel Emulsions. Once the one-phase regions were determined, different polymer/oil (P/O) ratios were essayed to determine the different amount of water solubilization in the reverse hexagonal and reverse cubic phases. Gel emulsions were prepared following two different paths: P/O = 90/10 for the formation of W/H_2 emulsions and 72.5/27.5 for W/I_2 (paths **a** and **b**, respectively, in Figure 1). Emulsions were prepared by weighing all components in the final concentration in dry glass tubes (ϕ = 13 mm). Then the samples were heated above the melting point of the I_2 and H_2 phases in order to reduce the viscosity of the system. Above the reverse structures melting point, a micellar solution is present instead of an ordered packed structure,[24] so the excess water could be mixed up to a complete homogenization of the emulsion by vigorous stirring in open air-cooling. Next, the samples were cooled down below the melting temperature in order to form the reverse structures around the water droplets and form the emulsions, which were kept at 25 °C until the SAXS or rheological analysis took place. With this method, gel emulsions could be formed. The determination of the transition temperature of the reverse structures is shown in further sections.

2.2.3. SAXS Measurement. Small-angle X-ray scattering (SAXS) measurements were used to confirm the I_2 and H_2 phases in liquid crystal samples and in gel emulsions and to determine phase boundaries. Measurements were performed in a SAXSess high-flux SAXS instrument (Anton Paar, Austria), operating at 40 kV and 50 mA. The X-ray source was a long-fine focus (LFF) sealed copper tube with horizontal line focus, which provided a radiation of wavelength 0.1542 nm. The sample−detector distance was 264.5 mm. Measurements were carried out under vacuum to prevent air scattering. The samples were filled with a syringe on refillable quartz capillaries (ϕ = 1 mm; sample volume = 1000 μL). The temperature of the samples was kept constant at 25 °C using a temperature controller. The scattered intensities were recorded with an imaging plate (IP) detection system, Cyclone (Perkin-Elmer), and via SAXSQuant software (Anton Paar), two-dimensional intensity data were converted to one-dimensional scattered intensities as a function of the scattering vector (q). The interlayer spacing of the liquid

crystal phases (d) was determined from the Bragg peaks obtained for every sample, using q, corresponding to the position of each reflection, following eq 1:

$$d = 2\pi/q \quad (1)$$

In the case of the reverse cubic phase, the lattice parameter (a) was calculated with the most intense reflection, as follows:[24]

$$a = (h^2 + k^2 + l^2)^{1/2} d \quad (2)$$

where h, k, and l are the Miller indices. The lattice parameter is also equal to the slope in the indexing of the peaks (d^{-1} vs $(h^2 + k^2 + l^2)^{1/2}$ plot).

For selected samples in the H_2 and I_2 phases, SAXS measurements were undertaken at temperatures between 20 and 85 °C to detect phase transition phenomena with increasing temperature and to confirm the results from the temperature ramp rheological tests.

2.2.4. Rheological Measurement. Rheological measurements were carried out in an AR-G2 rheometer (TA Instruments) using cone plate geometry (40 mm diameter, 1° angle, and 27 μm gap). Temperature was set and kept constant at 25 °C. A frequency sweep test (0.01−100 rad/s) was performed at a constant strain in the linear viscoelastic zone of the samples, which was determined previously in a strain sweep test. The elastic modulus (G') and the viscous modulus (G'') of samples were determined as well as the complex viscosity ($|\eta^*|$). Yield stress (τ_0) was determined with a stress sweep test: the inflection point in the shear rate versus shear stress plot was taken as the τ_0 value.

All measurements were carried out as a function of water concentration in the H_2 and I_2 zones, at P/O ratios of 90/10 and 72.5/27.5, respectively (paths **a** and **b** in Figure 1). Liquid crystal samples were prepared and homogenized at least 48 h before the measurement took place. Emulsion samples measurements took place within 24 h after their preparation. A sample cover was used to minimize the change in composition by evaporation during the analysis.

The temperature dependence of G', G'', and $|\eta^*|$ in selected samples of the reverse liquid crystals formed was determined with temperature ramp tests, from 10 to 60 °C in the linear regime (ω = 1 Hz, 0.5% strain) at a constant heating rate of 1 °C/min. These tests, together with SAXS measurements, were used to determine the temperature in which the order−disorder transition took place between different lyotropic mesophases and study the thermal behavior of the samples.

2.2.5. Differential Scanning Calorimetry (DSC). A differential scanning microcalorimeter (EXSTAR 6000, DSC6200, Seiko Instruments) was used to measure DSC of the samples at a heating rate of 10 °C/min. Samples were sealed in hermetic capsules, and an empty one was used as a reference.

3. RESULTS AND DISCUSSION

3.1. Phase Behavior of the Water/$(EO)_5(PO)_{68}(EO)_5$/Cyclohexane System at 25 °C. More than 100 samples were used to determine the phase behavior of the ternary system water/$(EO)_5(PO)_{68}(EO)_5$/cyclohexane at 25 °C. Cyclohexane was soluble in all proportions with the block copolymer P-121. The ternary phase diagram in weight fractions of the three components is shown in Figure 1. It can be observed that there are two anisotropic phases, the lamellar (L_α) phase and the reverse hexagonal phase (H_2); two isotropic phases, namely reverse-micellar cubic phase (I_2) and reverse micellar solution phase (L_2). Reverse phases, with negative interfacial mean curvature, are formed since the volume fraction of the hydrophobic part of the polymer is much higher than the hydrophilic part, so the critical packing parameter (CPP) is higher than one. The phase boundaries (±2.5 wt %) are represented as solid lines. The rest of the diagram corresponds to aqueous solutions in equilibrium with the one-phase zones.

The sequence of the phases formed, starting from the oil/copolymer binary axis to the water/copolymer binary axis is $L_2 \rightarrow I_2 \rightarrow H_2 \rightarrow L_\alpha$ (sphere, cylinder, plane), which corresponds to a change of curvature from negative to zero, is a consequence of the balance between the interfacial energy and the elastic energy per polymer chain when water concentration increases and oil decreases, so hydration of the hydrophilic part is enhanced and the critical packing parameter decreases down to one. When the copolymer concentration is low, it exists as simple unimers. When the concentration increases, they form aggregates, named micelles. At a higher concentration and with addition of water, the micelles grow and get closer to each other, and repulsive intermicellar interactions become more important. In order to maximize their distance, the micelles arrange into a reverse cubic lattice, which formation is also induced by the high volume fraction. If copolymer concentration is increased, it is observed that cylinder aggregates are formed, packed in a hexagonal lattice. Eventually, the curvature is changed to zero, forming a lamellar phase, at higher water concentration. Once the lamellar phase is achieved, the short PEO blocks in the unbalanced PEO−PPO−PEO block copolymer get saturated with water and further normal structures are not formed, in agreement with the "truncated" sequence found in Svensson et al.[25] According to Svensson,[25] when a block is saturated, additional solvent is added to the bulk, but it does not influence the curvature of the PPO/PEO interface. This truncated chain behavior is similar to that of surfactants presenting a low HLB number, which are generally soluble in an oil phase.

3.2. Formation and Stability of W/I_2 and W/H_2 Gel Emulsions. Two P/O ratios were chosen to form the reverse water-in-oil gel emulsions: 90/10 for the based reverse hexagonal gel emulsions (W/H_2) and 72.5/27.5 for the emulsions with reverse cubic phase in the continuous phase (W/I_2). A large amount of water could be emulsified in the reverse liquid crystals; in W/H_2 emulsions, up to 88 wt % of water could be incorporated as the internal phase and up to 93 wt % in the case of W/I_2 emulsions. In the range 80−93 wt %, a long mixing time combined with heating and centrifugation was required. In order to form gel emulsions above 93 wt % of internal phase, the idea of first forming the I_2 and H_2 phases and adding water gradually combined with continuous vortex stirring and heating was essayed, but unfortunately, the further added water was separated out as an excess water phase.

The emulsions formed, in both cases, were white due to the difference between the internal and external phase refractive index,[6,16] highly viscous, stiff, and presented shear-thinning behavior, and a yield stress value. They did not flow when the tube was turned upside down. The presence of liquid crystal phase in the continuous phase was confirmed with SAXS and rheological measurements. As the phase diagram depicts (Figure 1), and considering the components used, the structure of the liquid crystal is assumed to be reverse. Diluting the samples in cyclohexane, and not being able to dilute them in water, confirmed that the internal phase was indeed water. When observed through an optical microscope, small droplets in a highly packed structure were observed (data not shown). In the case of highly concentrated emulsions, as the volume fraction of dispersed phase is higher than the maximum packing volume fraction of rigid homogeneous spheres, which is equal to 0.74 for undistorted monodisperse spheres, droplets were no longer spherical, but they were deformed against their neighbors and took the shape of a polyhedron, with a consequent increase in their surface

Table 1. Characterization of the One-Phase Regions in the Phase Diagram (Notations as in Figure *1*)

	composition range					
phase/structure	P/O (w/w)	water (wt %)	diffraction planes (Miller indexes)	relative positions of the peaks	interlayer spacing (d/nm)	lattice parameter (a/nm)
H_2	>85/15	18−43	[100] [110] [200] [211]	1:√3:2:√7	d_1 = 11.20−23.3[a]	
$I_2/Fd3m$	70/30−90/10	8−20	[111] [311] [620] [551]	1:1.9:3.6:4.1	d_2 = 13.2−18.2[b]	a = 36.7−60.4[b]
L_α	>97.5/2.5	37−42	[100] [200] [300] [400]	1:2:3:4	d_1 = 14.38[c]	

[a] Following path **a** in the one-phase region (P/O = 90/10, 18−43 wt % water). [b] Following path b in the one-phase region (P/O = 72.5/27.5, 8−18 wt % water). [c] P/O = 97.5/2.5, 40 wt % water.

area. A polyhedrical shape is obtained since it is the best geometric conformation to achieve the most densely and optimized close-packed structure.

Emulsions were very stable, compared to other similar systems.[15] After 2 months, no phase separation was observed in emulsions up to 70 wt % of water. Emulsions up to 85 wt % for the W/I_2 emulsions were stable for more than 45 days, and for more than 20 days for >90 wt %, whereas for the W/H_2 emulsions, which are less viscous, phase separation started after 2 weeks for emulsions up to 88 wt % of water. The enhanced stability in gel emulsions was due to two different phenomena. In the first place, since the continuous phase was formed by an ordered block copolymer microstructure with an extremely high viscosity, droplet coalescence and creaming were highly impeded. In the second place, block copolymers provide a steric stabilization to emulsions, since they adsorb in the water−oil interface and create a barrier for droplet coalescence.[26] These two phenomena resulted in the proved high stability of the gel emulsions formed up to 70 wt %. For highly concentrated emulsions, as the liquid crystal fraction was less, the two stabilizing effects diminished.

3.3. Characterization of the One-Phase Regions and Based Gel Emulsions. The main characteristics of the liquid crystals are shown in Table 1. Apart from visual observation, the structure of the liquid crystals was established by SAXS measurements. Representative samples in each region were used to obtain the diffraction patterns and resolve the Bragg peaks. This, together with the indexing of the peaks, confirmed the phases found.

3.3.1. Reverse Hexagonal Phase and W/H_2 Emulsions. Samples corresponding to H_2 phase had a glassy appearance; they were stiff and optically anisotropic, since they showed a bright birefringence when observed through cross polarizers. The H_2 phase was found very near the I_2 phase, which hampered the determination of phase boundaries in this region. A large amount of water was solubilized by the H_2 phase (43 wt %), and a large variation of the interlayer spacing within this region was observed (Table 1) (Figure A, Supporting Information). Figure 2 shows the diffraction pattern of a representative sample (25 wt % water, P/O = 90/10), in which the four Bragg peaks are clearly seen (indexing R^2 = 0.9997). Figure 2 also shows the SAXS patterns for the water addition path followed (**a**) up to 80 wt % water, in which the presence of H_2 in the continuous phase is confirmed, including in highly concentrated emulsions, since correlation peaks, which indicate the presence of interactions among aggregates, can be still identified. However, the number and intensity of the peaks are reduced as water fraction is increased, since the

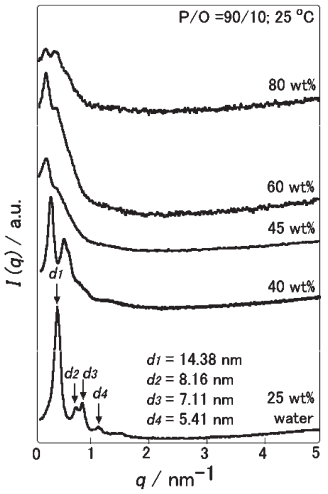

Figure 2. SAXS patterns of the water/$(EO)_5(PO)_{68}(EO)_5/C_6H_{12}$ system following path **a**, where the P/O ratio is fixed at 90/10, at 25 °C. The numbers above each curve are the weight fraction (wt %) of water in the samples. At 25 wt % water, the pattern corresponds to H_2 phase. The indexing of the peaks (Table 1) was performed, and a line passing through the origin was the best fit, with R^2 = 0.9997.

fraction of liquid crystal is less. It can be observed that the first Bragg peak, the one with the highest intensity, moves to lower q values as water concentration is increased in the H_2 phase, indicating water swelling of the aggregates (Figure A, Supporting Information). However, d remains constant (around 23 nm) in the W/H_2 emulsions, indicating phase separation of the excess water instead of solubilization. The intersection between the two lines was used to determine the phase boundary. The broad peak around q = 14 nm^{-1} in the wide-angle X-ray scattering (WAXS) was present in all samples.

Path **a** (Figure 1), with P/O = 90/10, was taken to study the formation of W/H_2 emulsions in this study. From 0 to 18 wt % water, there is a reverse micellar solution (L_2) and a mixed zone in which more than one phase coexist (L_2, I_2, and H_2). Between 18 and 43 wt % water, the one-phase region H_2 is present, and with further water addition, the gel emulsions could be formed up to 88 wt % of water.

3.3.2. Reverse Micellar Cubic Phase and W/I_2 Emulsions. A region of I_2 phase was found next to the reverse hexagonal H_2 phase and the reverse isotropic micellar L_2 phase. The maximum water solubilization was 20 wt % at P/O = 80/20. Just after preparing the samples at high temperature, in order to have the

L_2 phase and allow water swelling, the samples were white and turbid. They slowly turned into a stiff cloud appearance, when maintained at 25 °C, and after a few days, the samples in this region were transparent and with glassy appearance, very stiff, and they showed no birefringence when observed through cross polarizers as a consequence of their isotropy.

According to the relative positions of the Bragg peaks from a representative sample (10 wt % water, P/O = 72.5/27.5) (Figure 3) and to previous studies with similar systems,[16,21,25,27] the diffraction planes identified (Table 1) corresponded to the face-centered space group, *Fd*3*m*. This structure is supposed to be formed by 24 quasi-spherical reverse micelles, 8 of them larger and the other 16 smaller, as proposed by Luzzati and co-workers.[28] In reverse micelles, the repulsions between the PEO blocks are weak since they are in the core of the micelles, so a dense packed structure (face-centered) is favorable instead of a less dense packed body-centered structure, like most normal micellar cubic phases.[20] When preparing the liquid crystals, the transition from turbid to transparent was much slower for I_2 phase than for H_2 phase, which was in agreement with other studies that affirm that the kinetics of structuring and aging of the *Fd*3*m* phase is slow and takes ∼5 days to achieve fully transparency,[24] the time needed for water to incorporate in the two-sized micelle cores. Figure 3 shows the SAXS patterns along the water addition path followed (**b**), where P/O = 72.5/27.5 and W/I_2 emulsions are formed. It can be observed that in the I_2 phase region the two first peaks are the most intense and the second peak is clearly identified in the gel emulsions, even at high water concentrations, which confirmed the presence of a structured continuous phase up to 90 wt % water.

It is observed that the peaks shift to lower q values when the water concentration increases, which indicates that the interlayer spacing (d) and the lattice parameter (a) increased with increasing hydration of the reverse micelles forming the I_2 phase (Table 1) (values in the same order are found in the literature for similar systems).[18,25] The most intense reflection [311] was taken to calculate the interlayer distance and the lattice parameter. In the two-phase region, the interlayer distance and lattice parameter flattened at a value of 18.2 and 60.4 nm, respectively (Figure A, Supporting Information), as the excess water remained separated in microdomains, which resulted in the turbid aspect of the samples. Like in the H_2 phase, the intersection between the two lines was used to determine the phase boundaries, which corresponds to the full hydration point.

Path **b** (Figure 1), with P/O = 72.5/27.5, was taken to study the formation of W/I_2 emulsions in this study. From 0 to 8 wt % water there is a reverse micellar solution (L_2). Up to 18 wt %, the one-phase region I_2 is present, and with further water addition, the gel emulsions were formed up to 93 wt %.

3.3.3. Lamellar Phase, Reverse Micellar Solution Phase, and Multiphase Region. The transparency, softness, and birefringence characterized the one-dimensional lamellar structure, which swelled with only 2.5 wt % of cyclohexane. The diffraction patterns and indexing of a representative sample (40 wt % water, P/O = 97.5/2.5) can be observed in Figure B (Supporting Information) and peaks and d in Table 1.

The samples in the reverse micellar region (L_2) were transparent and isotropic, and they flowed when the tube was turned upside-down. When the polymer concentration was high, they were quite stiff, although they behaved as Newtonian fluids, as the viscosity was constant with frequency. The rest of the diagram is a two-phase or three-phase region, where in each

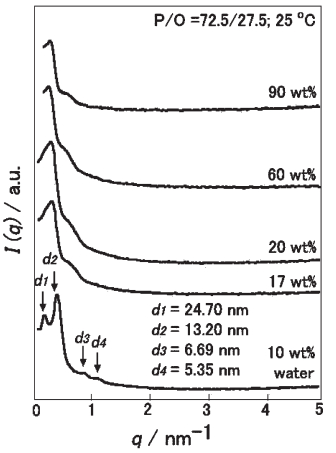

Figure 3. SAXS patterns of the $(EO)_5(PO)_{68}(EO)_5/H_2O/C_6H_{12}$ system following path **b**, where the P/O ratio is fixed at 72.5/27.5 at 25 °C. The numbers above each curve are the weight percent (wt %) of water in the samples. At 10 wt % water, the pattern corresponds to I_2 phase, structured as a face-centered space group, *Fd*3*m*. The indexing of the peaks was performed, and a line passing through the origin was the best fit, with $R^2 = 0.9995$.

point there is equilibrium between the one-phase regions, although these zones have not been investigated in detail. The W/H_2 and W/I_2 gel emulsions explained in the previous sections were formed in this region.

3.4. Transition Temperature and Thermal Behavior of the I_2 and H_2 Phases. The temperature at which the liquid crystals melt and the fluidity achieved facilitates the incorporation of water and the formation of emulsions has to be known in order to produce emulsions at higher scale. To evaluate the thermal evolution, visual observation, SAXS, and rheology tests were performed within the temperature range comprised between 10 and 80 °C, using two samples in the one-phase region at 25 °C. For the H_2 phase, 20 wt % water and P/O = 90/10 (sample A); for the I_2 phase, 12 wt % water and P/O = 72.5/27.5 (sample B).

Visually, sample A is stiff and transparent and shows birefringence at low temperatures. From 35 °C the birefringence disappears, indicating a phase transition to I_2 phase, since it continues stiff and transparent. From 45 to 50 °C, the sample appears white, indicating a phase separation, I_2 + W. At 60 °C, samples are no longer stiff, indicating that the liquid crystal has melted into a micellar solution, L_2 + W. Sample B has the typical appearance of an I_2 phase up to 35−40 °C; from this point the sample is cloud and flow under its own weight, indicating the melting of the cubic phase to L_2 + W. DSC measurements were performed to detect the phase transitions. However, the enthalpy associated with the phase transitions was very small, much smaller than those for direct liquid crystals, indicating that the interaction among reverse aggregates is much smaller than that for direct ones, as also observed in Rodríguez-Abreu et al.[18] Even though, it could be observed that the phase transition from a liquid crystal to a melted state took place at higher temperatures for sample A than for sample B (data not shown).

These visually detected changes were consistent with SAXS results. Figure 4 show the diffractograms from 30 to 80 °C for sample A. Up to 35 °C, the diffraction peaks indexing adjusts for a reverse hexagonal phase (Figure 5a), whereas between 40 and 50 °C, an *Fd*3*m* I_2 structure is detected at 50 °C (Figure 5b).

The interlayer spacing increases continuously from 20 to 35 °C in the H_2 phase (Figure C, Supporting Information);

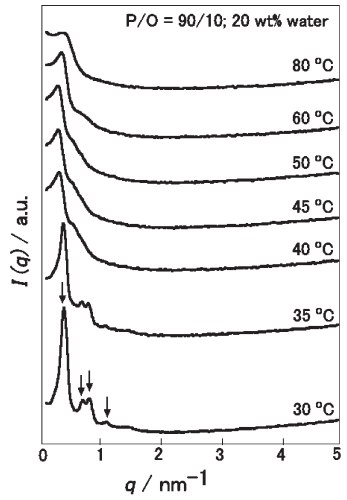

Figure 4. Temperature dependence of sample A (20 wt % water, P/O = 90/10) measured by SAXS after equilibration for 7 days at 25 °C. The different curves correspond to temperatures of 30, 35, 40, 45, 50, 60, and 80 °C. The results show a transition from the diffractogram of a H_2 phase below 40 °C to a characteristic diffractogram of a I_2 phase between 40 and 50 °C, to a L_2 diffractogram above 50 °C. Peaks indexed in Figure 5a are indicated with an arrow.

then a sudden increase is observed when the phase transition H_2—I_2 takes place, and it increases continuously in the I_2 region. The pass from H_2 to I_2 is consistent with the fact that with increasing temperature the block copolymer becomes more lipophilic, so a more negative curvature is favored.

SAXS patterns for sample B at 25 °C show the characteristic peaks for a reverse I_2 phase sample, and it can be detected up to 50 °C (Figure 6). This cubic phase was also identified as an *Fd*3*m* structure (Figure D, Supporting Information). The interlayer distance and the lattice parameter in this region increase with temperature (Figure E, Supporting Information), possibly due to the straightening of polymer chains, which are shrunk at lower temperatures. From 60 °C, with the melting of the cubic phase, the interlayer distance remains almost constant with temperature in the range studied. This point corresponds to the order—disorder transition, in which the packed ordered micelles become a reverse micellar solution.

The phase transition from H_2 to I_2 (sample A) and the melting of I_2 (sample B) observed visually and by SAXS was also observed through rheology tests. A temperature ramp rheological test was performed from 10 to 60 °C (local evaporating in the sample limited the temperature range in rheological experiments), and the viscoelastic parameters as well as the complex viscosity were measured. Figure 7 shows a temperature ramp test for samples A (a) and B (b). It can be observed that at low temperatures G' is higher than G'', since the liquid crystals have a solidlike structure.

For sample A, at low temperatures, $G' > G''$ but both increase gradually. At 31 °C there is a change of the slope of $\tan(\delta)$, which corresponds to the transformation of the anisotropic reverse hexagonal phase H_2 into an isotropic reverse cubic phase I_2 beyond that temperature. From this value, G' increases steeper and G'' starts to drop down. At 42 °C, G' and $|\eta^*|$ of this I_2 formed reach the highest values, whereas G'' experiments the lower values at the same moment. Then, at 52 °C, another inflection point in $\tan(\delta)$ indicates the beginning of the melting of the I_2 phase, and G' and $|\eta^*|$ suddenly drop. G'' increases up to

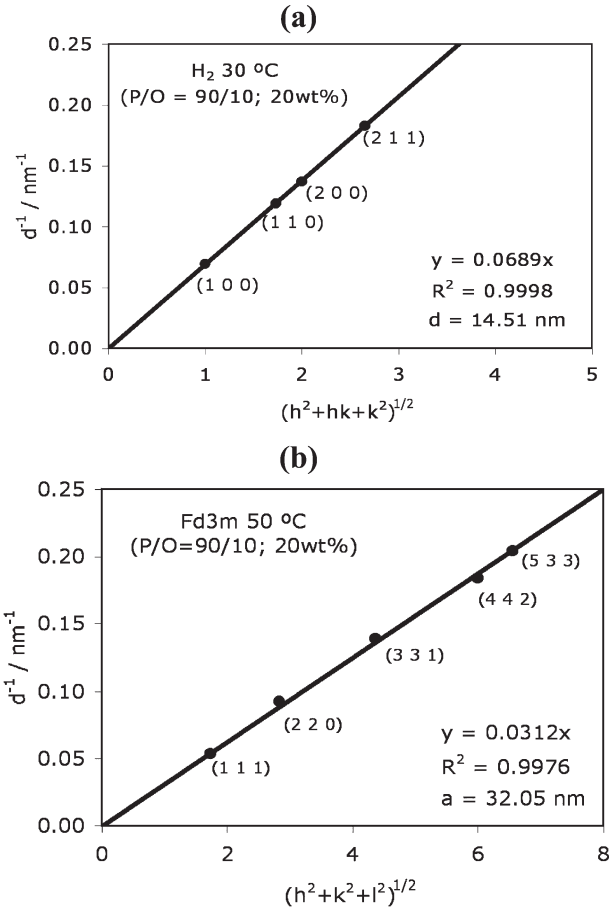

Figure 5. Indexing of the SAXS peaks of sample A (P/O = 90/10 and 20 wt % water). (a) At 30 °C (peaks indicated with an arrow). A H_2 structure is observed. (b) At 50 °C, where an *Fd*3*m* structure is observed.

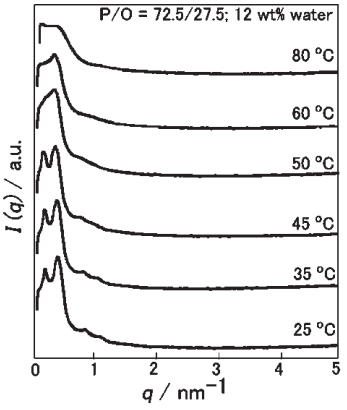

Figure 6. Temperature dependence of sample B (12 wt % water, P/O = 72.5/27.5) measured by SAXS after equilibration for 7 days at 25 °C. The different curves correspond to temperatures of 25, 35, 45, 50, 60, and 80 °C. The results show a transition from the diffractogram of an I_2 phase below 50 °C to an L_2 diffractogram above this temperature.

55 °C, as a consequence of the loss of the gel structure, and after the crossover between G' and G'' it also drops.

When temperature increases, for sample B, G' is constant until 36 °C, where it starts to decrease as it starts to melt into a reverse micellar phase. This transition is observed with a clear increase of the slope of $\tan(\delta)$ at this temperature. A crossover between G'

dx.doi.org/10.1021/la104539q |*Langmuir* 2011, 27, 2286–2298

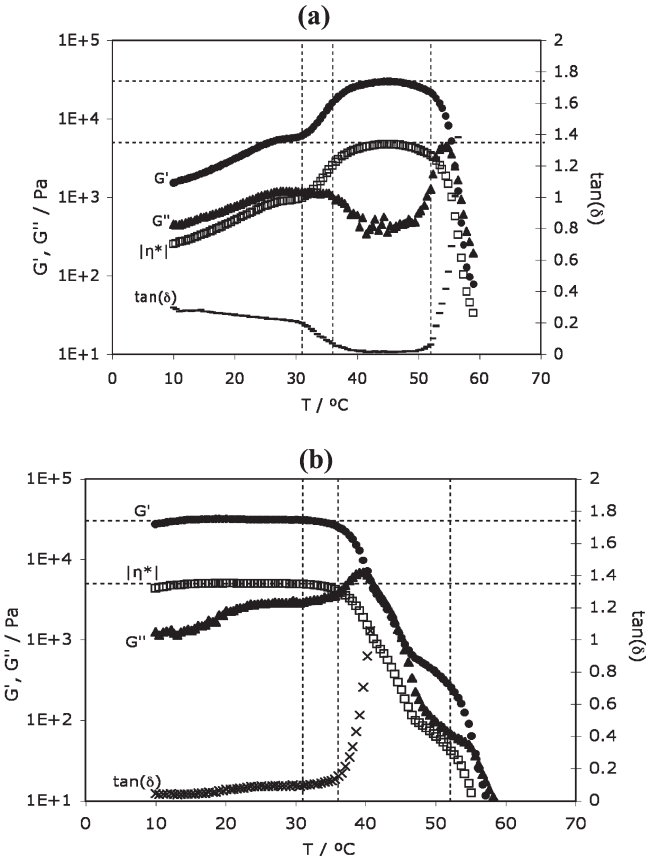

Figure 7. (a) Temperature ramp test for sample A (20 wt % water, P/O = 90/10) and (b) for sample B (12 wt % water, P/O = 72.5/27.5). Test conditions: $\omega = 1$ Hz and 0.5% strain. The diagram shows the complex viscosity ($|\eta^*|$, □), the elastic (G', ●), and the viscous (G'', ▲) modulus, and $\tan(\delta) = G''/G'$ (—, ×), as a function of temperature.

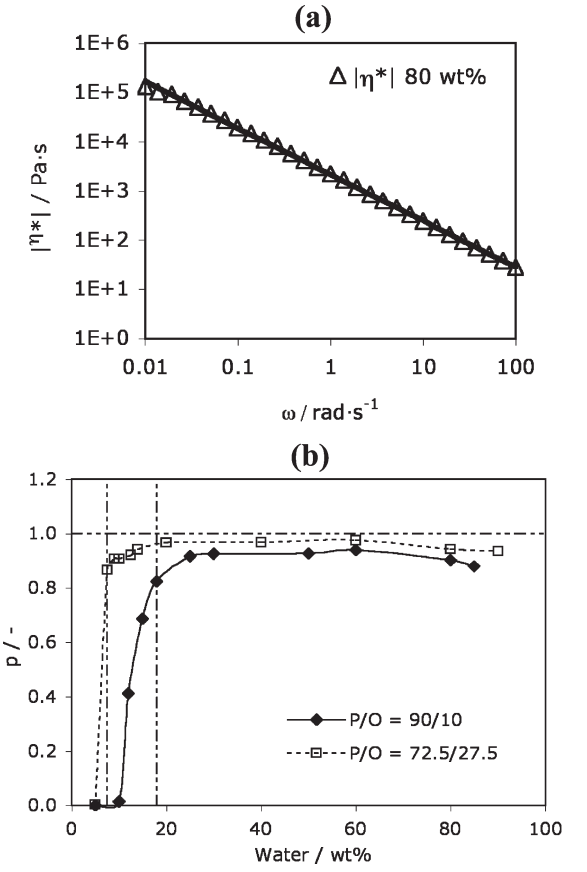

Figure 8. (a) Fitting of the complex viscosity (Δ) as a function of frequency with a power law ($|\eta^*| \sim \omega^{-p}$). Sample at P/O = 72.5/27.5 and 80 wt % water. (b) Exponent of the power law (p) as a function of water weight percent following path a (◆) and path b (□); p → 1 indicates a solidlike substance, whereas p → 0 indicates liquid behavior. The lines are only a guide for the eyes.

and G'' takes place at 40 °C, which is followed by a steep decrease in both values, when the sample behaves as a liquid. The complex viscosity follows the same pattern: it is high and constant at low temperatures, until it reaches the melting point, and then it suddenly drops.

The optimum temperature for emulsification corresponds to the temperature in which the viscosity is lower. At lower temperatures, the viscosity is still high and the mixing would require a higher energy input in order to mix the excess water with the liquid crystal structure. According to Kunieda et al.,[29] the melting temperature of the one-phase regions increases as water is solubilized in the reverse micelles until phase separation occurs, and it is maximum in the two-phase region, so higher temperatures are needed to form the gel emulsions.

3.5. Rheological Properties of the Liquid Crystals and Gel Emulsions at 25 °C. Oscillatory linear viscoelastic experiments were performed, since they give us information about the liquid crystals and gel emulsions' structure and behavior under stress without damaging the internal structure, as small deformations are applied. The viscoelastic parameters and the yield stress were evaluated as a function of increasing water concentration at 25 °C, at two fixed P/O following path **a** (90/10) and **b** (72.5/27.5) shown in Figure 1.

3.5.1. Viscoelastic Parameters of the Reverse Phases and Based Gel Emulsions at 25 °C. All samples have a typical shear-thinning behavior, as observed in the example of Figure 8a, since the complex viscosity ($|\eta^*|$) decreases with increasing frequency, and no plateau region at low frequencies is observed. $|\eta^*|$ is higher than 10^5 Pa·s (at $\omega = 0.01$ rad/s) in the I_2 phase and than 10^4 Pa·s in the H_2 phase. The complex viscosity can be fitted to a power law model, $|\eta^*| \sim \omega^{-p}$, where the exponent ($p$) indicates a solidlike structure when approaching one or a liquid behavior when it is close to 0.[30] When $p = 0$, the viscosity is constant with frequency (Newtonian behavior). Figure 8b shows the value of this exponent as a function of water concentration for the two water addition paths followed in this study. For path **a**, the exponent is near 0 up to 10 wt % water and then increases at values higher than 0.9 and remains nearly constant all along the path. For path **b**, there is a steeper increase of the exponent in the disorder−order transition at <10 wt % water, and the exponent presents values near 1 in the I_2 phase and in W/I_2 gel emulsions. In both cases, the results indicate that in the micellar solutions zone the sample behaves like a liquid, but from the moment that the liquid crystal is formed and with further addition of water, even at high concentrations, the samples have a solidlike behavior, which is mainly due to the structured continuous phase, either I_2 or H_2.

Since there is no plateau value, the viscosity is plotted, just for comparison, as a function of water content at 0.1 rad/s in Figure 9 (open symbols). For path **a**, the viscosity is low until the H_2 phase is formed, at 18 wt % water, where a sudden increase in viscosity

dx.doi.org/10.1021/la104539q |*Langmuir* 2011, 27, 2286–2298

is observed. From that point, the viscosity decreases with a constant slope with further water addition up to 80 wt %, from where the viscosity reduction is more important. For path **b**, first, a sudden increase in viscosity of 5 orders of magnitude can be observed when the disorder−order transition takes place, from the reverse micellar solution to the reverse cubic phase at 8 wt % water. The viscosity of the reverse cubic phase is so high, since it consists of a close-packed structure, involving polymer chain interpenetration and adhesive interactions between micelles. The viscosity of the samples in the cubic phase region is nearly constant, and in the two-phase region it decreases down to 10^4 Pa·s at 90 wt % water. The $|\eta^*|$ of the I_2 phase is higher than that of the H_2 phase; as a consequence, gel emulsions formed with the reverse cubic phase in the continuous phase are more viscous than those formed with the reverse hexagonal phase, at a constant water concentration.

In emulsions in which there is no liquid crystal in the continuous phase, the behavior is the opposite: the viscosity and the elastic modulus increase as the disperse phase concentration increases, from diluted emulsions to highly concentrated ones.[31] In that case, the viscosity of the emulsions is mainly determined by the volume fraction of dispersed phase: as it increases, a tighter and close-packed network is formed, with droplets touching one another. In our case, the liquid crystal phase is the responsible for the high viscosity of the emulsions, so when the internal phase fraction is increased, the liquid crystal phase fraction decreases, and so does the viscosity. This was also observed in other similar systems[15] with O/I_1 emulsions.

The rheograms of both I_2 and H_2 phases and based gel emulsions are characteristic of gel type substances presenting a non-Newtonian shear-thinning behavior. The elastic modulus (G') is higher than the viscous modulus (G'') in all the frequency range studied (0.01−100 rad/s), indicating the elastic nature of the samples. G' increases gradually until a plateau value is achieved, although it is nearly frequency-independent in all the samples studied, which evidence the gel-type structure of the liquid crystals and the emulsions formed. In path **a**, the frequency crossover is observed from 12 to 18 wt % (at concentrations below the H_2 region) and for path **b** between 7.5 and 12.5 wt %. For higher water concentrations there is no crossover in the frequency range studied, which indicates, on the one hand, that the structural relaxation times are very high, characteristic of gels and, on the other hand, an increase of the relaxation time with increase of the dispersed phase concentration. The G'' in the H_2 phase and W/H_2 gel emulsions present a shallow minimum at frequencies near 1 rad/s (Figure 13). In the I_2 phase, the G'' variation with frequency was found to be that of a polymeric liquid, with a broad peak at low frequencies followed by a relaxation process with a bulk relaxation time equal to $\tau = 1/\omega_{max}$, being ω_{max} the frequency where the G'' peak is found (Figure 10).

G' and G'' are higher in the I_2 phase (on the order of 5×10^4 Pa) than in the H_2 phase. The values of G' are comparable to other studies[18,24] in which an *Fd*3*m* space group in a reverse micellar cubic phase is found. The value of the G^* for the reverse phases and gel emulsions is nearly frequency-independent.

As the microstructure of the continuous phase is responsible for the elastic nature of the samples, contrarily to the two-liquid concentrated emulsions, the Princen−Kiss equations,[32,33] valid for highly concentrated emulsions in which G' is predicted to increase with dispersed phase concentration, cannot be applied here. This can be observed in Figure 9, where G' (ω = 100 rad/s)

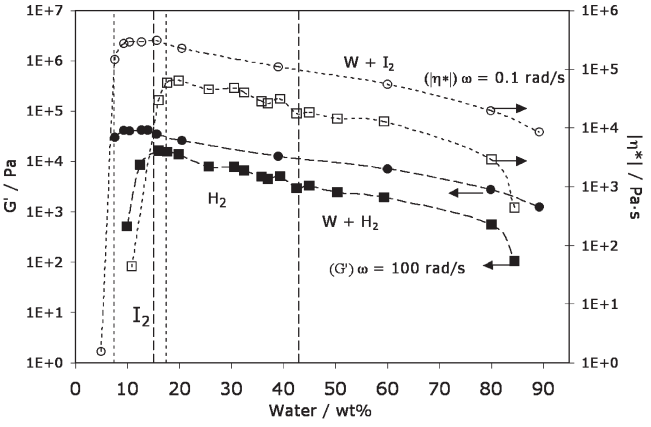

Figure 9. Elastic modulus at ω = 100 rad/s (G', filled symbols) and complex viscosity at ω = 0.1 rad/s ($|\eta^*|$, open symbols) as a function of water weight percent following path **a** (P/O = 90/10; ■, □) and path **b** (P/O = 72.5/27.5; ●, ○). Temperature is 25 °C. Other notations as in Figure 1. The lines are only a guide for the eyes.

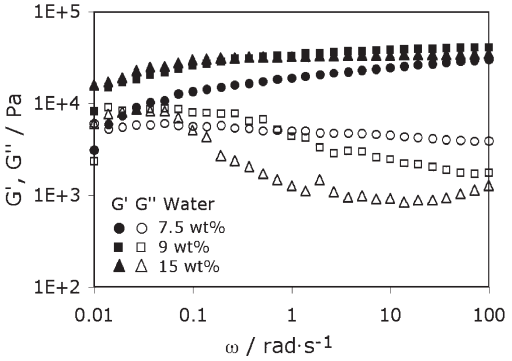

Figure 10. Frequency sweep test data of the elastic (G') (filled symbols) and viscous (G'') (open symbols) modules of the I_2 phase at 25 °C at three different water weight fractions, as indicated. P/O is fixed at 72.5/27.5 (path **b**).

is represented as a function of water weight fraction (filled symbols) for path **a** and **b**. Despite the continuous decrease of G' along the whole water addition paths, since the volume fraction of liquid crystal is reduced, in the I_2 one-phase region there is a small increase in the G' values as the samples are more hydrated, and the highest G' value is found in the phase boundary, as it has also been observed in similar studies[33] with a direct cubic phase.

In the reverse micellar solution region, $G' < G''$ in all the frequency range, and both G' and G'' increase with frequency as well as G^*.

3.5.2. Modeling the Viscoelastic Parameters. The viscoelastic properties of the reverse liquid crystals and based gel emulsions cannot be described with the well-known Maxwell equations. Other models are needed to describe the experimental data in the linear viscoelasticity zone to be able to achieve good theoretical predictions. In this study, in order to provide a link between rheology and the microstructure of the reverse hexagonal (H_2) and cubic (I_2) phases and based reverse gel emulsions (W/H_2 and W/I_2), the fitting of the viscoelastic data was evaluated in order to find a model that could describe them. However, three different theories were needed: the cooperative flow model from Bohlin,[35] the soft glass rheology (SGR) model for soft materials,[36,37] and the slip plane theory for cubic phases.[38] These models have

dx.doi.org/10.1021/la104539q |*Langmuir* 2011, 27, 2286–2298

been used previously in several studies regarding the rheology of cubic and hexagonal phases and based gel emulsions[4,17,39] and for gels formed with different surfactants,[40,41] so they seemed appropriate to be used in the present system.

Theory of Cooperative Flow. This theory was presented by Bohlin[35] to explain the flow character and microstructure of a flowing substance by means of rheological data. This theory supposes that a flowing substance is divided into several flow units that are responsible of the macroscopic flow observed, which is only the consequence of their cooperative rearrangements (active cooperative flow). These flow units are meant to be recognizable and identified in the microstructure of the substance, such as atomic or molecular aggregates. In dynamic experiments, the theory of cooperative flow states that the complex modulus and the frequency are related by the following expression:

$$G^*(\omega) = \sqrt{G'(\omega)^2 + G''(\omega)^2} = A\omega^{1/z} \qquad (3)$$

where $G^*(\omega)$ is the complex modulus, $G'(\omega)$ and $G''(\omega)$ are the elastic and viscous modulus, respectively, ω is the frequency, A represents the interaction strength between the flow units, and z is the coordination number of cooperative flow units in the structure, which provides an indication of the substance microstructure. The two parameters of the theory can be determined from experimental data. The theory is valid, according to Bohlin,[35] in the range of frequencies corresponding to times between the relaxation time (τ) and the stationary state. In colloidal systems, such as liquid crystals mesophases, Bohlin[35] affirms that the coordination number in flow coincides with the coordination number in the colloidal structure, which is equal to 2 for a lamellar structure, 6 for a close-packed rod hexagonal structure, and 12 for a close-packed cubic structure. In fact, for a cubic structure it could vary between 6 (simple cubic structure), 8 (body-centered structure), or 12 (face-centered structure).

From the dynamic data obtained in oscillatory experiments the coordination number (z) can be estimated with reliability at $\omega \leq \tau^{-1}$, that is, at frequencies below the frequency where the crossover between G' and G'' takes place. However, this theory has been applied in many systems[34,42] in which $G' \gg G''$ in all the frequency range. This theory has been used to determine the interaction among aggregates and crystalline domains in hexagonal liquid crystals with nonionic surfactants and block copolymers,[17,34] in reverse hexagonal liquid crystals with block copolymers,[17] in CTAB/water mixtures,[40] and also in food preparations like jam or yoghurt.[42] The values for the normal hexagonal phase (H_1) vary considerably from ~3 to 9.5 in different systems.[15,17,40] The values for H_2 are reported[17] as ~6.7. The main cause of this mismatch could be that in all of the systems studied there was no crossover between G' and G'' since the samples were gel-type.

For path **a**, the experimental values show a good fitting to eq 3 in all the range studied, from 5 to 85 wt % water, and parameters A and z could then be estimated. As it can be observed in Figure 11 (filled symbols), G^* is highly dependent on frequency in the micellar zone (10 wt %), whereas in the H_2 phase and W/H_2 emulsions it is nearly frequency independent, reaching the highest values at 20 wt % water. From that point, G^* decreases with water fraction. The same model was also used to fit the experimental data corresponding to the water addition path **b**, in which W/I_2 emulsions are formed between 20 and 93 wt % water (Figure 11, open symbols). In this case, the fitting was excellent for the samples with low water concentration (5 wt %), where the

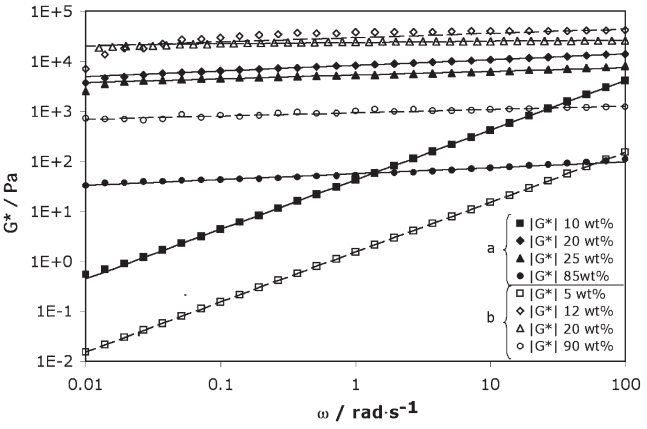

Figure 11. Dynamic complex modulus (G^*), as a function of frequency for selected samples in path **a** (filled symbols, P/O = 90/10) and path **b** (open symbols, P/O = 72.5/27.5) with increasing amount of water. The lines show the fitting of experimental data (points) to eq 3, $G^* = A\omega^{1/z}$ (Bohlin theory) (path **a**, continuous line; path **b**, dashed lines).

reverse micellar phase is present and for the highly concentrated W/I_2 gel emulsions, ≥ 80 wt %. However, for the samples in the reverse cubic phase range and in the more diluted emulsions, a good fitting could not be obtained (path b, 12 and 20 wt % in Figure 11), since the G^* did not follow a power law function. Therefore, for this path, the parameters A and z are only reliable when the amount of liquid crystal is low or inexistent (micellar solution, $z \approx 1$, and at 90 wt % water, $z \approx 15$, consistent with the presence of a cubiclike structure).

By a minute examination of the definition of the complex viscosity ($|\eta^*|$)

$$|\eta^*| = |G^*|/\omega \qquad (4)$$

one can observe that when combining eq 3 and eq 4, and at $\omega = 1$ rad/s, $|\eta^*| = |G^*| = A$; so, $\eta^*(\omega = 1 \text{ rad/s}) = A$. That is, the interaction strength parameter and the complex viscosity at 1 rad/s of frequency have the same value. The overlapping can be observed in Figure 12, where the complex viscosity at 1 rad/s and the parameter A are plotted as a function of water concentration following path **a** (filled symbols) and **b** (open symbols). At low water concentrations the values are low; they suddenly increase in the one-phase region and, from that point, gradually decrease as water concentration is increased. The fact that A is equivalent to $|\eta^*|$ at 1 rad/s along the entire water addition path indicates that the interaction strength between flow units strongly determines the viscosity of the system. To our knowledge, this is the first time that this direct association between the complex viscosity and the interaction strength parameter is performed, and we believe that it helps a better understanding of the cooperative flow theory. As it happened with complex viscosity, the interaction strength in the reverse cubic phase emulsions is higher than in the reverse hexagonal phase in the continuous phase, suggesting that the interaction force between reverse micelles that conform the reverse cubic phase is stronger than that of reverse cylinders that conform the hexagonal phase.

The coordination number (z) for path **a** is also plotted in Figure 12 (filled squares). The coordination number is close to unity in the reverse micellar solution zone, since the reverse micelles do not form an entangled network and they behave as Newtonian fluids. The coordination number increases with concentration in the non-Newtonian region, until it reaches a

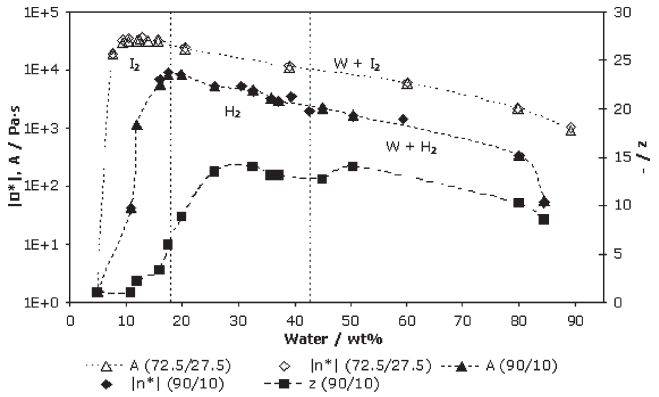

Figure 12. Complex viscosity ($|\eta^*|$) at ω = 1 rad/s (◆, ◇, Δ), interaction strength coefficient (A, ▲), and coordination number (z, ■) for path **a** (P/O = 90/10) as a function of water weight fraction and for path **b** (P/O = 72.5/27.5; $|\eta^*|$, ◇; A, Δ).

constant value around 13 in the H_2 phase, which is higher than those found in the literature,[15,17,40] as seen before. When water concentration is further increased and the gel emulsions are formed, z remains almost constant along the whole water addition path, since it is basically determined by the continuous phase structure, although there is a slight decrease in the higher concentrated emulsions due to the increased amount of excess water between the mesophase. It can be observed that when the coordination number is higher, the dynamic complex modulus, G^*, is more frequency independent, since the slope $(1/z)$ is smaller. This indicates that when the coordination number between the different aggregates or domains is high, the substance resembles a gel-type structure with flow units strongly attached, whereas when the aggregates do not form an entangled network (low z values), the system is fluid, less viscous and G^* strongly depends on frequency.

Soft Glassy Rheology (SGR) Model. This model was introduced by Sollich[36,37] and is applicable to many soft materials, like emulsions and foams. The model creates an analogy between the rheology of these materials and glassy dynamics, since they have a disordered structure like a liquid, but the stiffness of a solid. They are characterized for being composed of different aggregates that are maintained together due to weak interactions, and they can remain in metastable states in a disordered configuration for a long period of time. Apart from being soft materials, their elastic (G') and viscous (G'') modules have weak or negligible frequency dependence and a nearly constant ratio (G''/G').

The theory states that in these materials each element is trapped in energy wells or cages,[43] formed due to the interactions with the elements that surround it, like cross-links or energy bindings. In normal glasses, the elements hop from one well to another when temperature is increased, but in this case, the elements cannot escape from their well only with thermal motion, since the energy barriers to overcome are too high. An extra motion is needed, named random agitation or noise temperature (x), which is caused by the coupling effect within the system that can excite an element in a metastable state and bring it to another. The energy that is released from a rearrangement in one point of the system is propagated to another point and causes the hopping of the elements, as an analogy to the activation energy needed to initiate a chemical reaction.

The model exhibits some limitations. The most relevant one is that it assumes that x is a constant parameter in the model. Moreover, the predictions are only physically relevant in the low frequency range $(\omega \leq 1)$, since fast local stress relaxation processes are neglected in front of the more drastic ones. However, it has the advantage that the predictions can be made by only determining one parameter, the noise temperature (x). This parameter is part of the exponent (Δ) of the power law used to describe the elastic and viscous modules (eqs 5, 6, and 7):

$$G' \approx \omega^{\Delta}; \quad \Delta = x - 1 \tag{5}$$

$$G'' \approx \omega^{\Delta}; \quad \Delta = x - 1 \tag{6}$$

The movement between wells depends on the trap depth and on the noise temperature. When $x > 1$, there is enough agitation to induce the moving or flow of the elements between the wells, and the system is in constant movement and disordered. Even though, the interactions are too weak to bring the system to an ordered, stable, less energy state, so the system cannot achieve a complete structural relaxation. The system is in continuous state of remodeling and changing its configuration, with its elements hopping from one metastable state to another. When $x \rightarrow 1$ $(\Delta \rightarrow 0)$, random agitation decreases and the elements become trapped in deeper wells; G' and G'' become more frequency independent. When $x = 1$, the glass transition is achieved, and the system behaves like an elastic solid. When $x > 3$, the system follows the Maxwell model at low frequencies.

The model also expects, as long as the frequency is higher than the crossover frequency, that G'' can decrease as ω increases, so in this case $x < 1$ and the power-law exponent would be negative. This is in agreement with some experimental results,[41] which found this behavior of G'' in the low-frequency range in liquid crystalline gel systems. In this case, G' was predicted to be constant.

This model was used to fit the experimental data from the two water addition paths (**a** and **b**) with fixed P/O ratio. In the case of micellar solutions (<10 wt % for path **a** and <8 wt % for path **b**), the model fitted well the experimental data, even with the same x for both G' and G'' (although the fitting error was smaller when x was different for the two modules). In the case of P/O = 90/10, in the H_2 phase and W/H_2 emulsions, the model was good for the elastic modulus (G'), but not for the viscous modulus (G''), when maintaining x constant (Figure 13), and if it was different, G'' was well fitted at low frequencies, with $x < 1$ (Figure 13). We encountered a similar behavior as in Nair et al.,[41] in which G'' presents a shallow minimum, so it cannot be described by a simple power-law model. We propose that the behavior of G'' could be described by two noise temperatures (x_1 and x_2). On the basis of the concept that the SGR model also takes into consideration that an equilibrium state can also exist for $x < 1$, when G'' increases as the frequency decreases at very low frequencies, one noise temperature would be smaller than 1 $(x_1 < 1)$, in order to have the negative slope of G'', whereas there would be a higher random agitation or noise temperature $x_2 > 1$ at higher frequencies. Both values would be close to 1, since they are typical of gel-like substances. Therefore, the second noise temperature, x_2, apart from the existing parameter x (now x_1) was introduced in the model, to obtain the following expression:

$$G'' \approx (\omega^{x_1 - 1} + \omega^{x_2 - 1}) \tag{7}$$

It has to be noted that if $x_1 = x_2$, then $x_1 = x_2 = x$, and the model returns to its original form, with only one parameter, and the system can be described by the power-law behavior. A good

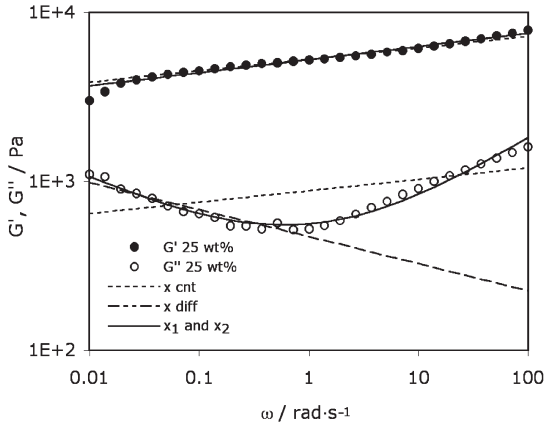

Figure 13. Fitting of the soft glass rheology (SGR) model for a sample in path **a** (P/O = 90/10) and 25 wt % water for G' (●) and G'' (○) as a function of frequency. Thin dashed line: constant x for both G' and G'' (G' and $G'' \sim \omega^{x-1}$; $G'' \sim \omega^{x-1}$). The model does not fit well for G''. Thick dashed line: different x for G′ and G″ ($G' \sim \omega^{x-1}$; $G'' \sim \omega^{x-1}$). The model fits up to 1 rad/s for G″. Continuous line: one x for G′ ($G' \sim \omega^{x-1}$) and x_1 and x_2 for G″ ($G'' \sim \omega^{x_1-1} + \omega^{x_2-1}$). The model fits well the experimental data.

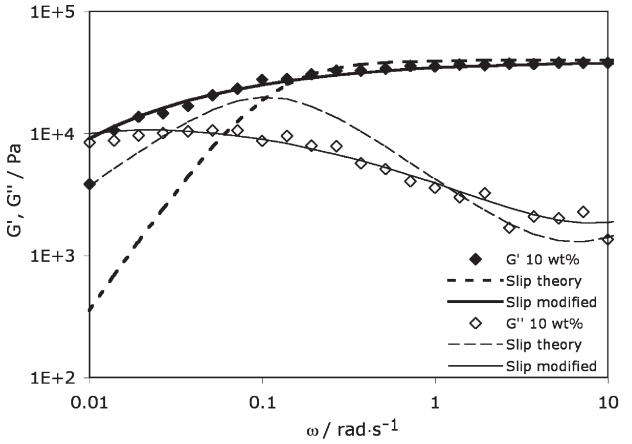

Figure 14. Elastic modulus, G' (♦), and viscous modulus, G'' (◇), as a function of frequency for samples with fixed P/O = 72.5/27.5 at 10 wt % water, corresponding to I_2 phase. The lines show the fitting of experimental data (points) to the Slip theory (eqs 8 and 9) (dashed) and modified slip theory (eqs 11 and 12) (continuous). Thick lines for G' and thin lines for G''.

fitting of the modified model is obtained in the whole frequency range for path **a**, when G'' is described by two noise temperatures (Figure 13).

In path **b**, apart from the micellar solution, the modified model fitted well the samples corresponding to the W/I_2 emulsions, above 20 wt % of water, but the I_2 one-phase region could not be described by this model, as G'' and G' had a more complex behavior, so another model is needed to describe the rheological behavior of the I_2 phase.

"Slip Planes" Model for Colloidal Systems. This theory was developed by Jones and McLeish[38] to describe the frequency dependence of the storage and loss modulus of cubic phases. However, they suggest expanding their theory to general weak solids. The theory assumes that when stress is applied to a cubic phase sample, its structure rearranges itself in planes that are aligned parallel to the shear plane. The shear stress acts tangentially to the planes, and as it increases, it causes the deformation of the sample by sliding along the planes, causing a displacement between the different layers. The deformations in the slip plane are very high, whereas the deformation of other planes is maintained low.

As it is a relaxation process, the theory includes the fact that at low shear stress the sample has a solidlike behavior, but from a critical stress value, it relaxes and behaves as a liquid. The behavior of the sample is only linear when no slips exists; above a critical strain, slippage appears and the samples are in a pseudolinear behavior, and the complex modulus, apart from depending on frequency, depends also on strain. This theory only involves the flow of the liquid, not the rupture and forming of new bonds. The components of the complex modulus in this case are calculated as follows:

$$G'(\omega) = GA\,\frac{\omega^2\tau^2 - \omega^2\tau\tau_L}{1+\omega^2\tau^2} \qquad (8)$$

$$G''(\omega) = GA\,\frac{\omega\tau(1+\omega^2\tau\tau_L)}{1+\omega^2\tau^2} \qquad (9)$$

where ω is the frequency, τ_L is the local relaxation time, which is calculated as $\tau_L = \tau_{min}^2/\tau$, where τ_{min} is the inverse of the frequency where G'' reaches the minimum value. G is the bulk stress modulus, and $A = \eta' N/(\eta + \eta' N)$, where η is the bulk viscosity, η' the slip plane viscosity, and N the number of slipping planes in the crystal. GA can be estimated as one single parameter, since in this case, as N is very high, $A \rightarrow 1$.

However, by calculating G' and G'' with eqs 8 and 9, the calculated values deviated considerably from the experimental data (Figure 14, dashed lines). So, according to Rodríguez-Abreu et al.,[4] based on Maestro et al.,[44] instead of having a unique value of the relaxation time, a log-normal distribution of τ was used (eq 10).

$$H(\tau) = \frac{1}{\sigma\sqrt{2\pi}}\exp\left(\frac{(\ln(\tau_i) - \ln(\tau_c))^2}{-2\sigma^2}\right) \qquad (10)$$

where σ is the logarithmic standard deviation, $\tau_c = 1/\omega_c$, and ω_c is the frequency of the crossover between G' and G''. If no crossover is observed in the frequency range studied, the value of 0.01 rad/s is taken to calculate the log-normal distribution for the relaxation time. To calculate G' and G'', then, the following equations were used:

$$G'(\omega) = \sum_{\tau_i} H(\tau_i)GA\,\frac{\omega_i^2\tau_i^2 - \omega_i^2\tau_i\tau_L}{1+\omega_i^2\tau_i^2} \qquad (11)$$

$$G''(\omega) = \sum_{\tau_i} H(\tau_i)GA\,\frac{\omega_i\tau_i(1+\omega_i^2\tau_i\tau_L)}{1+\omega_i^2\tau_i^2} \qquad (12)$$

As it can be observed, a unique value of τ_L was taken, which was obtained by fitting eq 8 and 9 to the experimental data. In this modified slipping model, only the parameters GA and σ were determined by fitting eqs 11 and 12 to the experimental G' and G'', such that the average square deviation between calculated and experimental data was minimum (least-squares fit) (ω: 1, 2, ..., n):

$$\sum_{i=1}^{n}\left(\left[\frac{G'_{exp}(\omega_i)}{G'_{calc}(\omega_i)} - 1\right]^2 + \left[\frac{G''_{exp}(\omega_i)}{G''_{calc}(\omega_i)} - 1\right]^2\right) = \min \qquad (13)$$

Figure 14 shows the fitting of the slip planes model to the experimental data for G' (◆) and G'' (◇). As it can be observed,

dx.doi.org/10.1021/la104539q |*Langmuir* 2011, 27, 2286–2298

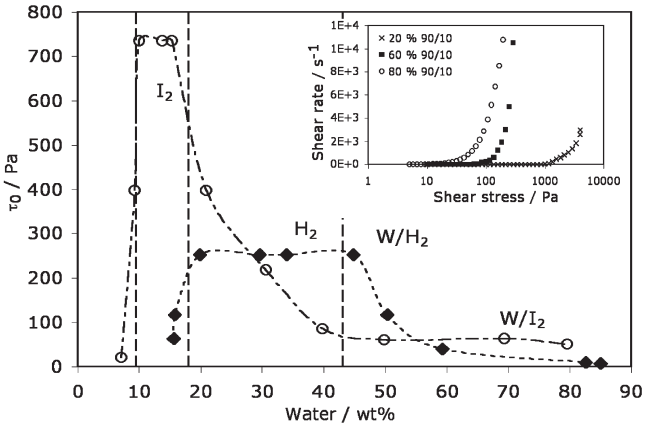

Figure 15. Yield stress values as a function of water weight fraction following the two paths (P/O = 90/10, path **a**, ♦), and (P/O = 72.5/27.5, path **b**, ○) at 25 °C. Inset: rheogram (shear rate versus shear stress) for samples at a fixed P/O = 90/10 (path **a**) and different water concentrations (20 (×), 60 (■), 80 wt % (○)) showing the non-Newtonian behavior as the relationship between both parameters is nonlinear. Other notations as in Figure 1.

the modified slip plane theory model (continuous line) fitted considerably well with the experimental data, especially for the elastic modulus (thicker line). For the G'' the model fitted much better than the other models seen here, although at $\omega > 10$ rad/s the deviations from the experimental data were considerable, and a perfect fitting in the range 0.01−10 rad/s was still not achieved. However, at present, it is the best theory that describes the viscoelastic parameters special behavior of the cubic phase structures and has been used in other similar studies in reverse cubic phases[4,17] and in lamellar liquid phase.[39]

3.5.3. Yield Stress of I_2 and H_2 Phases and Based Gel Emulsions. The yield stress (τ_0) was calculated for samples following the water addition paths (**a** and **b**) of Figure 1 in steady-state flow rheological analysis. As shown in the inset of Figure 15, samples with a water concentration above the order−disorder transition are non-Newtonian fluids, as they do not exhibit a linear relationship between shear rate and shear stress. A certain threshold value must be overcome to initiate flow, which is equal to the yield stress of the samples, so their behavior can be fitted with a Herschel−Bulkeley[45] model, $\tau = \tau_0 + k\gamma^n$, where τ is the shear stress and γ is the shear rate and k and n the fitting parameters. As observed in Figure 15, the yield stress values for paths **a** and **b** are constant in the one-phase region and then gradually decrease with water fraction, as the volume fraction of the liquid crystal is reduced, so for the most highly concentrated emulsions, the yield stress has the minimum value. Again, this is the opposite behavior of normal two-liquid emulsions.

The yield stress values for the I_2 phase are much higher than for the H_2 phase, as it also happened with the complex viscosity and the elastic and viscous modulus.

4. CONCLUSIONS

The present study was focused on the phase behavior and rheological analysis of the water/$(EO)_5(PO)_{68}(EO)_5$/C_6H_{12} system. The formation of reverse phases was observed and confirmed by SAXS analysis as well as the formation of highly stable gel emulsions with a structured reverse liquid crystal in the continuous phase (H_2 and I_2 phase), which were formed up to high water fractions (88 and 93 wt %, respectively). This is the first time, to our knowledge, that highly concentrated W/H_2 gel emulsions were formed and characterized with SAXS and rheology. It was observed that the stability of these emulsions was indeed very high, and at the highest concentrations, the stability of W/I_2 was higher than that of W/H_2. This difference in stability is related to the fact that the elastic behavior, complex viscosity, and yield stress values were lower for W/H_2 than for W/I_2 gel emulsions.

The thermal analysis of the I_2 and H_2 phase showed that I_2 melted to a reverse micellar phase with excess water and that the H_2 phase experienced an increase on the G' and $|\eta^*|$ corresponding to a phase transition to a I_2 phase with a more negative curvature, which eventually melted at a higher temperature.

The analysis of the rheological data was performed in order to obtain one model that could describe not only the experimental results of the liquid crystals but also the ones of the highly concentrated emulsions. However, three models were needed to fit the rheological data of the samples and relate it with their microstructure. With the Bohlin theory, which fitted the G^* to a power-law model, the H_2 phase and W/H_2 emulsions could be described. Moreover, it was useful to understand the microstructure of the samples as indicated with the coordination number, which was characteristic of the fluid elements structure, and the interaction strength parameter, which was seen to be strongly related with the viscosity of the system. The soft glass rheology (SGR) model was then applied and needed to be modified; another parameter was introduced to explain the behavior of the G''. With two noise temperatures, the model fitted well the experimental data in the H_2 phase and in the gel emulsions with I_2 and H_2 in the continuous phase. However, to explain the viscoelastic results of the I_2 phase, the slip plane theory seemed the most appropriate; although instead of only one relaxation time, a log-normal distribution of relaxation time was indeed needed to fit the experimental data correctly. We expect, in further studies, to obtain a single model that could describe the rheological data of all the systems.

Additionally, the fact of using block copolymers as emulsifiers opens the possibility to further studies, regarding the formation of meso/macroporous materials and nanoparticles, due to the interesting and varied aggregation and rheological properties that these offer.

■ ASSOCIATED CONTENT

Supporting Information. Figures A−E. This material is available free of charge via the Internet at http://pubs.acs.org.

■ AUTHOR INFORMATION

Corresponding Author

*Phone +34 9340 39789. Fax +34 9340 21291. E-mail anna.may@ub.edu.

■ ACKNOWLEDGMENT

This study would not have been possible without the financial support from the Spanish Ministry for Science and Innovation (MICINN) within the framework of the project CTQ2008-06892-C03-03/PPQ. A. May is grateful to MICINN for the grant received to perform a stay in Yokohama National University (Japan).

REFERENCES

(1) Kunieda, H.; Solans, C.; Shida, N.; Parra, J. L. *Colloids Surf.* **1987**, *24*, 225–237.
(2) Rodríguez, C.; Shigeta, K.; Kunieda, H. *J. Colloid Interface Sci.* **2000**, *223*, 197–204.
(3) Hamley, I. W. *Block Copolymers in Solution: Fundamentals and Applications*; John Wiley & Sons, Ltd.: Chichester, 2005.
(4) Rodríguez-Abreu, C.; Garcia-Roman, M.; Kunieda, H. *Langmuir* **2004**, *20*, 5235–5240.
(5) Mele, S.; Murgia, S.; Monduzzi, M. *Colloids Surf., A* **2003**, *228*, 57–63.
(6) Uddin, M. H.; Rodríguez, C.; Watanabe, K.; Lopez-Quintela, A.; Kato, T.; Furukawa, H.; Arracima, A.; Kunieda, H. *Langmuir* **2001**, *17*, 5169–5175.
(7) Rodríguez-Abreu, C.; Lazzari, M. *Curr. Opin. Colloid Interface Sci.* **2008**, *13*, 198–205.
(8) Esquena, J.; Solans, C. In *Emulsions and Emulsion Stability*; Sjoblom, J., Ed.; Taylor & Francis: Boca Raton, FL, 2006; Chapter 6.
(9) Esquena, J.; Izquierdo, P.; Kunieda, H.; Solans, C. *Proceedings of the 1st Iberian Meeting on Colloids and Interface*, Salamanca, 2005.
(10) Rodríguez-Abreu, C.; Esquena, J.; Aramaki, K.; Lopez-Quintela, M. A. *Microporous Mesoporous Mater.* **2009**, *119*, 338–343.
(11) Chae, W.-S.; Braun, P. V. *Chem. Mater.* **2007**, *19*, 5593–5597.
(12) Rodríguez-Abreu, C.; Lazzari, M.; Varade, D.; Kaneko, M.; Aramaki, K.; Lopez-Quintela, M. A. *Colloid Polym. Sci.* **2007**, *285*, 673–680.
(13) Kresge, C. T.; Leonowicz, M. E.; Roth, W. J.; Vartuli, J. C.; Beck, J. S. *Nature* **1992**, *359*, 710–712.
(14) Uddin, M. H.; Kanei, N.; Kunieda, H. *Langmuir* **2000**, *16*, 6891–6897.
(15) Alam, M. M.; Sugiyama, Y.; Watanabe, K.; Aramaki, K. *J. Colloid Interface Sci.* **2010**, *341*, 267–272.
(16) Watanabe, K.; Kanei, N.; Kunieda, H. *J. Oleo Sci.* **2002**, *51*, 771–779.
(17) Rodríguez-Abreu, C.; Aramaki, K.; Kunieda, H. *Colloids Surf., A* **2005**, *269*, 59–66.
(18) Rodríguez-Abreu, C.; Shresta, L. K.; Varade, D.; Aramaki, K.; Maestro, A.; Lopez, A.; Solans, C. *Langmuir* **2007**, *23*, 11007–11014.
(19) Rodríguez, C.; Uddin, Md. H.; Watanabe, K.; Furukawa, H.; Harashima, A.; Kunieda, H. *J. Phys. Chem. B* **2002**, *106*, 22–29.
(20) Alexandridis, P.; Olsson, U.; Lindman, B. *Langmuir* **1996**, *12*, 1419–1422.
(21) Alexandridis, P.; Olsson, U.; Lindman, B. *Langmuir* **1998**, *14*, 2627–2638.
(22) Angelico, R.; Ceglie, A.; Olsson, U.; Palazzo, G. *Langmuir* **2000**, *16*, 2124–2132.
(23) Shigeta, M.; Murgia, S.; Ceglie, A.; Monduzzi, M.; Ambrosone, L. *Colloids Surf., A* **2003**, *228*, 57–63.
(24) Pouzot, M.; Mezzenga, R.; Leser, M.; Sagalowicz, L.; Guillot, S.; Glatter, O. *Langmuir* **2007**, *23*, 9618–9628.
(25) Svensson, B.; Olsson, U.; Alexandridis, P. *Langmuir* **2000**, *16*, 6839–6846.
(26) Alexandridis, P. *Curr. Opin. Colloid Interface Sci.* **1996b**, *1*, 490–501.
(27) Alexandridis, P.; Olsson, U.; Lindman, B. *Langmuir* **1997**, *12*, 23–34.
(28) Luzzati, V.; Vargas, R.; Gulik, A.; Mariani, P.; Seddon, J. M.; Rivas, E. *Biochemistry* **1992**, *31*, 279–285.
(29) Kunieda, H.; Uddin, Md. H.; Horri, M.; Furukawa, H.; Harashima, A. *J. Phys. Chem. B* **2001**, *105*, 5419–5426.
(30) Silioc, C.; Maleki, A.; Zhu, K.; Kjøniksen, A.; Nystrom, B. *Biomacromolecules* **2007**, *8*, 719–728.
(31) Pal, R. *Food Hydrocolloids* **2006**, *20*, 997–1005.
(32) Princen, H. M.; Kiss, A. D. *J. Colloid Interface Sci.* **1986**, *112*, 427–437.
(33) Princen, H. M.; Kiss, A. D. *J. Colloid Interface Sci.* **1989**, *128*, 176–187.
(34) Alam, M. M. Formation and rheological behavior of hexagonal and cubic phase based gel emulsions. Ph.D. Thesis,Yokohama National University, Sept 2009.
(35) Bohlin, L. *J. Colloid Interface Sci.* **1980**, *74*, 423–434.
(36) Sollich, P.; Lequeux, F.; Hebraud, P.; Cates, M. E. *Phys. Rev. Lett.* **1997**, *78*, 2020–2023.
(37) Sollich, P. *Phys. Rev.* **1998**, *58*, 738–759.
(38) Jones, J. L.; McLeish, T. C. B. *Langmuir* **1995**, *11*, 785–792.
(39) Németh, Z.; Halasz, L.; Palinkas, J.; Bota, A.; Horanyi, T. *Colloids Surf., A* **1998**, *145*, 1047–119.
(40) Coppola, L.; Gianferri, R.; Nicotera, I.; Oliviero, C.; Ranieri, G. A. *Phys. Chem. Chem. Phys.* **2004**, *6*, 2364–2372.
(41) Nair, G. G.; Prasad, S. K.; Bhargavi, R.; Jayalakshmi, V.; Shanker, G.; Yelamaggad, C. V. *J. Phys. Chem. B* **2010**, *114*, 697–704.
(42) Gabriela, D.; de Cindio, B.; d'Antona, P. *Rheol. Acta* **2001**, *40*, 120–127.
(43) Weeks, E. R.; Weitz, D. A. *Phys. Rev. Lett.* **2002**, *89*, 095704−1–095704−4.
(44) Maestro, A.; González, C.; Gutiérrez, J. M. *J. Rheol.* **2002**, *46*, 127–143.
(45) Sherman, P. *Industrial Rheology*; Academic Press: New York, 1970; pp 97−321.